Hydroxyethyl Cellulose-Based Electrically Conductive Mechanically Resistant Strain-Sensitive Self-Healing Hydrogels

Imtiaz Hussain (imtiazhussain@njfu.edu.cn)
Nanjing Forestry University
Xiaofeng Ma
Nanjing Forestry University
Linlin Wu
Nanjing Tech University
Zhenyang Luo
Nanjing Forestry University

Research Article

Keywords: wearable strain sensors, self-healing, hydrogel, natural polymer, electronic skin

Posted Date: September 22nd, 2021

DOI: https://doi.org/10.21203/rs.3.rs-901296/v1

Abstract

Mechanical self-healing and pressure sensitivity are the two most important features of human skin. An electrically conducive and versatile material, which can replicate auto-healing and sense mechanical strength, can be used in different areas, including biomimetic prostheses and robotic technology. It is still a difficult challenge to combine all these properties into one material. In this article, we report a self-healing sensor with iron (III) metal ions, which shows a mechanical stable, auto-healing, and conductive properties at room temperatures. Different concentrations of natural polymer and iron (III) can be used to tune mechanical strength and electrical conductivity. The hydrogel will reach stress of 0.51 MPa, a fracturing strain of 1250%, and electrical conductivity of 2.21×10^{-1} Sm^{-1}. The engineered hydrogel also exhibits flexion and pressure response, indicating that it is a good candidate for electronic skin applications.

Introduction

Flexible and self-repairing ability of the human skin permits its function as a defensive barrier while being exposed to continuous diminishing, even though incessantly detecting the external environment. A supreme biomimetic electronic sensor skin should exhibit analogous mechanical sensing and repeatable self-healing proficiencies. Like human skin, both sensors and electrodes must have repeatable mechanical and self-healing capability at the damage places at ambient temperature. Although electronic skins are approaching human skin-like properties and performance in terms of mechanical sensing, their repeatable self-healing capability is very rare in electronic skin sensors (Tee et al. ; Lipomi et al. 2011; Someya et al. 2004; Pang et al. 2012). The intrinsic self-healing and mechanical sensing ability of the electronic skin sensors will be useful in various emerging fields, including soft robotics, health detections, wearable electronics, tissue engineering, and stretchable bioelectronics (Xu et al. 2019; Kim et al. 2019; Yu et al. 2021).

In recent years, various strategies for the fabrication of electronic skin have been reported, including the use of nanoclay (Xin et al. 2016), inorganic nonmetallic nanocomposite (Wang et al. 2019b; Qin et al. 2020), metal nanoparticles (Zhu et al. 2019; Zeng et al. 2019), and conductive polymers (Wang et al. 2018b; He et al. 2019; Chen et al. 2019). Although most of them showed high sensitivity and low hysteresis, their poor mechanical stretchability, self-recovery, and conductivity limit their potential applications in electronic devices (Zhang et al. 2019a; Sarwar et al. 2017). Bielawski et al. reported an organometallic polymer-based self-healing conductive thin film, exhibited a very low conductivity (10^{-3} Scm^{-1}) and the healing ability was shown in organic solvent at high temperature (Williams et al. 2007). Combining high bulk electrical conductivity, repeatable self-healing, and force sensitivity remains a challenge in the fabrication of strain sensors. Several strategies have been reported for the development of flexible electronic materials. Among them, hydrogels are the promising candidates because of their flexible, biocompatible, stretchable, self-recoverable, and healing nature (Zhang et al. 2019b; Liao et al. 2017; Li et al. 2018; Wang et al. 2019a; Amoli et al. 2019; Yu et al. 2019). The electrical performance of these hydrogels can be improved by integrating with a conductive filler, such as graphene, carbon

nanotubes, conductive polymers, metal nanowire, and metal cations(Wan et al. 2018; Guo et al. 2010; Wang et al. 2018a). Hydrogel-based strain sensors can be used to detect relative resistance and capacitance change caused by variation in shape upon external forces (Zhou et al. 2019; Lei and Wu 2018). The aqueous phase of the hydrogel 3D network enables them to dissolve ions, which act as ion transporters to transmit electrical signals(Cao et al. 2017). Because of the lack of dynamic intonation, conventional hydrogels suffer from poor mechanical performance, limiting their potential applications(Calvert 2009). Thus, designing stable hydrogels with outstanding mechanical, self-healing, and high bulk electrical conductivity properties is important in the fabrication of smart, portable, and wearable electronic devices(Feig et al. 2018). To fabricate tough hydrogel by introducing an effective dissipation mechanism, many efforts have been reported in past decades, such as nanocomposite hydrogels(Wang et al. 2012), double-network hydrogels(Gong et al. 2003), nanostructured hydrogels(Xia et al. 2013), slide-ring hydrogel(Okumura and Ito 2001), polyampholytes hydrogels(Sun et al. 2013a), and microsphere composite hydrogel(Huang et al. 2007). The incorporation of noncovalent interactions, such as ionic bonding(Sun et al. 2013b), metal-ligand interactions(Kean et al. 2014), hydrogen bonding(Xu et al. 2017; Kushner et al. 2007), hydrophobic association(Hao et al. 2013), supramolecular interactions(Kakuta et al. 2013), molecular diffusion, and chain entanglement(Zhang et al. 2012), enhance the mechanical strength and self-healing performance of the hydrogels. The elasticity and mechanical strength of hydrogels can be improved by increasing the physical cross-linking density, which reduces ion migration and lowers their conductivity (Depalle et al. 2015; Shin et al. 2016). Hydrogel should possess both high mechanical strength and good conductivity for their use in stretchable sensors and artificial tissue applications. Therefore, the balanced elasticity, elongation and mechanical strength mimic human tissue with high bulk conductivity are important for hydrogel materials for their commercial applications in various fields (Gong et al. 2003; Zhou et al. 2019). Odent et al. reported ionic gels with 2.9 Sm^{-1} electrical conductivity, 425% strain, very low tensile strength, and elasticity of 0.007 MPa and 5 kPa, respectively (Odent et al. 2017). Zhou et al. also reported a dual-cross-linked hydrogel, in which Fe^{3+} was introduced into a PAAm-co-PAAc hydrogel network to establish ionic coordination. These hydrogels showed considerable elongation and self-healing properties (Lin et al. 2015). Lidong and coworkers recently reported gelatin based self-healable and stretchable hydrogel strain sensor *via* hydrogen bonding and hydrophobic interactions showing 95% self-healing efficiency (Wang et al. 2019a). Qiming et al. also reported mussel-inspired nanocomposite (TA/PANI@CNCs) hydrogel strain sensor, that exhibits 974% elongation strain, 759 kPa fracture stress, room temperature self-healing ability, good conductivity, and strain sensitivity properties (Yan et al. 2020).

In this study, we successfully fabricated a high-strength, ultra-stretchable, and self-healable electronic sensor based on ionic conductive hydroxyethyl cellulose polyvinyl alcohol/PAA-Fe^{3+} (HEC-PVA/PAA-Fe^{3+}) hydrogels. HEC was used to prepare an ionically conductive hydrogel sensor with a dual cross-linked structure that includes ionic coordination among PAA-Fe^{3+}, HEC-Fe^{3+}, and hydrogen bond interaction between the HEC-PVA polymer chain and HEC-PAA polymer network. Polyvinyl alcohol (PVA) was used as a physical cross linker to form more hydrogen bonds due to the higher number of –OH groups on its linear polymer chain. The binding motifs (-COO^-) of PAA to the metal ion (Fe^{3+}) make a physically cross-

linked network that plays a vital role in the good conductivity of the hydrogel sensor, based on the novel composition and multiple cross-linked network structures. The fabricated HEC hydrogel-based sensor exhibited robust mechanical properties, such as ultrastretchability, high strength, toughness, elasticity, and self-recovery. In this work, we have investigated whether varying the concentration of polymers and metal ions would affect the material properties and self-healing activity of the resulting hydrogel or not. We used hydroxyethyl cellulose, polyvinyl alcohol, acrylic acid, and iron (III) metal ions that spontaneously formed stable hydrogels on mixing. We optimized the concentration of various polymers and metal ions, which resulted in the formation of hydrogels with high strength, high self-healing efficiency, and conductive properties. By comparing the stress-strain strength, we found that the hydrogel with the concentration of HEC (4%), PVA (10%), AA (3 mL), and Fe^{3+} ion (0.20 M) showed the maximum tensile strength, self-healing efficiency, and high ionic conductivity.

Materials And Methods

Materials

Hydroxyethyl cellulose (HEC) (CELLOSICE™ QP 15000) was purchased from DOW chemical company. Acrylic acid (AR > 99%), ferric chloride hexahydrate and initator ammonuim persulphate (RG ≥ 98%) were provided by the Shanghai Macklin Biochemical Co. Ltd. Polyvinyl alcohol (PVA) (1750 ± 50) was purchased from Sinopharm Chemical Reagent Co. Ltd., Shangai. The purification of AA was carried out by the process of vacuum distillation. All the solutions were prepared in deionized water.

Fabrication of hydrogels.

Hydrogels were prepared by a two-step process of free radical polymerization at room temperature followed by a freeze-thaw cycle. Firstly, hydroxyethylcellulose-poly (vinyl alcohol) (HEC-PVA) solutions with different concentration ratios were prepared in deionized water. Specifically, 5,10 & 15% PVA solutions were prepared by dissolving a calculated amount of PVA in DI water at 95□C and cooling them to 60□C slowly under continuous stirring. Thereafter, various amounts of HEC were added to the above solutions to make the HEC concentrations of 2, 3, 4 & 5% in the mixture and kept them at this temperature for 2 hours under continuously stirring. Afterward, the obtained HEC-PVA solution was stirred at room temperature for a few hours to remove the bubble and marked them solution A. Acrylic acid (AA) (2, 3 & 4 mL) was charged to 5 mL solution of A and stirred at room temperature to form a homogeneous mixture. The obtained mixture was treated with various concentrations (0.05, 0.10, 0.20, 0.40 & 0.80 M) of iron (III) chloride hexahydrate aqueous solution, followed by the addition of 1 mL initiator APS aqueous solution (1mg/mL) and stirred it for another10 minutes to form a homogeneous mixture. The mixture was transferred to glass tubes followed by a process of sonication to remove the bubbles and keep them at room temperature for the construction of the first network of hydrogels by a free radical polymerization reaction. Further, hydrogels were frozen in a freezer for 8 hours followed by thawing at room temperature for 8 hours to form a second network, and this cycle was repeated three times. Finally, these hydrogels

were subjected to different tensile and compression tests to find their mechanical properties and used for the monitoring of various human motions.

Characterization

The formation of hydrogel and M-L coordination was confirmed by using the Nicolet 5700 FTIR spectrometer in the range of 4000 – 500 cm^{-1}. Freeze-dried hydrogel samples in powder form were mixed with KBr under hydraulic pressure to form a uniform pellet and the spectra of hydrogel samples were recorded at room temperature. Both the tensile and compression tests were performed by using (CMT4501) universal tensile testing machine. Tensile strength samples were made in a rectangular shape with a dimension of 2 × 4 × 30 mm, compression strength samples were made in a cylindrical shape with a diameter of 20 mm and a height of 12 mm. The cross-head speed for measuring the tensile strength was 60 mm/min, and that for compression strength it was 2.0 mm/min. The self-healing performance was recorded macroscopically and equated the relative tensile strength of the healed and original hydrogel samples with different constituents content at different healing times. The percent self-healing efficiency (SHE) was calculated as a proportion of tensile strength restored to the tensile strength of the original hydrogel sample. Electrochemical impedance spectroscopy (EIS) was applied to measure the ionic conductivity of the hydrogel. A thin membrane of 1mm in thickness and 12 mm in radius was used for measuring the ionic conductivity of the hydrogel sensor. Electrochemical workstation CH1660E and CMT2103 electrochemical tensile testing machines were used to record the real-time electrical signals at different strains. A constant voltage of 2.0 V was used during the whole process and the real-time signal was recorded by using the amperometric i-t curve program. The relative changes in resistance ($\Delta R = R-R_0/R_0$), based on fixed applied voltage to the strain sensors and variation in the electrical signal under various strains were calculated by the Ohm's Law ($R = U/I$).

Results And Discussion

Fabrication of hydrogel

The construction of a physical double network strategy in hydrogel networks generally improves their mechanical performance and self-recovery efficiency. Based on this concept, we engineered a natural polymer-based (HEC) double network hydrogel sensor with robust mechanical, self-healing, and conductive properties. Figure 1 shows the schematic diagram for the fabrication of HEC-PVA/PAA-Fe^{3+} hydrogels *via* free radical polymerization of the first network and freezing-thawing cycles for the construction of the second network. Firstly, the HEC-PAA solutions of different concentration ratios were prepared at different temperatures, and then various concentrations of AA were added to the pre-cooled HEC-PAA solution under continuously stirring. After the formation of the homogeneous mixture, various molar concentrations of Iron (III) hexahydrated chloride were added to the obtained mixture and followed by the addition of APS solution. The formation of hydrogels was carried out at room temperature followed by the freezing-thawing cycles. Owing to the abundance of oxygen-containing groups on the polymer chain, such as carboxyl, hydroxide, and ether groups, as well as metal ions, the development of

numerous non-covalent associations occurred concurrently in the hydrogel network. The majority of the hydroxyl groups in hydroxyethyl cellulose and polyvinyl alcohol form intermolecular and intramolecular hydrogen bonds, which help to keep the hydrogel network stable. The ethyl oxygen and carboxylic groups of PAA form an ionic coordination interaction with a tri-positive ferric cation (Fe^{3+}), which plays an important role in the hydrogel network's self-healing performance. Besides, hydrogen bonding might also form in the HEC and PAA network between the –OH groups of HEC with the $–COO^-$ and –OH groups of PAA. All these binding interactions were confirmed by FTIR spectroscopic technique.

The FTIR spectra of the pure HEC, HEC/PAA-$Fe^{3+,}$ and the hydrogel sensor HEC-PVA/PAA-Fe^{3+} is shown in Fig. 1. The absorption peaks at 3450 and 2932 – 2862 cm^{-1} in the HEC spectrum are due to the presence of stretching vibrations of –OH and –CH bonding in the HEC polymer. The absorption bands at 1186 cm^{-1} represent the C-O bond stretching, while the band at 1049 cm^{-1} shows the deformation of the O-H bond and the bands in the fingerprint region are due to C-H bond bending vibrations. The disappearance of C-H stretching and narrowing of O-H stretching in the HEC/PAA-Fe^{3+} spectrum confirm the involvement of these groups in metal coordination and hydrogen bond formation. The change in the fingerprint region also confirms the formation of non-covalent bond formation in the HEC/PAA-Fe^{3+} hydrogel materials. The spectrum of the strain sensor hydrogel HEC-PVA/PAA-Fe^{3+} shows clear cut differences both in the functional group region and fingerprint region. The most significant change is in the O-H stretching vibration field, which has widened, implying that more –OH groups are involved in the hydrogel materials as a result of the addition of PVA.

This broad region also confirms the formation of the metal-ligand bond between the –OH groups and metal cations. The band at 1754 cm^{-1} also confirms the formation of coordination bonds among metal ions and carboxylate ions in the hydrogel network. The disappearance of certain peaks in the fingerprint region also confirms the formation of hydrogen and metal-ligand coordination bonds in the strain sensor hydrogel materials.

Compression analysis

The compression strength of the hydrogel samples with different PVA concentrations in cylindrical shape was performed at a cross-head speed of 2mm/min by using (CMT4501) universal tensile testing machine. All the hydrogel sensors were capable of enduring compression above 98% fracture strain. The fracture stress, fracture strain, fracture toughness, and compression modulus (0–30% strain) were determined from the corresponding compressive stress-strain graphs (Fig. 2a). The compressive stress-strain curves for the HEC hydrogel sensor containing PVA 5%, 10% & 15% are shown in Fig. 2a. It can be seen from Fig. 2c, that all the hydrogel sample curves exhibit a linear behavior at initial strain percent and from which we can calculate the modulus of the hydrogel sensors. The compression stress of the hydrogel sensor increases slightly with increasing deformation and achieved about 28 MPa compression stress irrespective of their different PVA concentration. These phenomena indicate that these hydrogels could be compressed completely without any fracture, which confirms their 3D tough network nature. The hydrogel sensor has a higher maximum compression stress (28 MPa) than pure hemicellulose-based

hydrogels. These hydrogels, however, have shown different strain percentages and a hydrogel with a 10% PVA level is able to resist the high compression of ~ 100%. High PVA content formed a brittle hydrogel network causing a decrease in the compression strength including compression strain (%), toughness, and compression modulus. The PVA content showed a trend of the first increase and then decrease in compression strain, compression modulus, and compression toughness. This indicates that with low PVA content the number of hydrogen bonds was less as compared to the optimized concentration (10%) of PVA, while higher concentration results in a brittle network due to the formation of extra crosslinking in the hydrogel network.

In this study, we investigated the effect of PVA concentration on the compression modulus and the strain percent (0–30%) was selected for the comparison of their modulus strength. Compression modulus is an important parameter for the measurement of the strength of hydrogel materials and it was calculated by dividing stress by strain percent. As shown in Fig. 2c & d, the compression modulus of the hydrogel sensor increased as the concentration of PVA increased from 5–10%, while a further increase in PVA% content results in a decrease in the compression modulus. This indicates that optimum PVA concentration could promote a maximum number of inter and intra hydrogen bonds that stiffen the hydrogel network structure. This indicates that the incorporation of PVA polymer affects the mechanical strength of the hydrogel network.

Tensile strength.

The mechanical properties of the hydrogel sensor were characterized *via* a uniaxial tensile testing machine (CMT4501) with a crosshead speed of 60 mm/min at room temperature. The tensile stress-elongation tests were performed quantitatively and we found that the mechanical strength of the hydrogels was significantly influenced by HEC concentration, PVA concentration and iron (III) ions Fe^{3+} molar concentration. The mechanical properties of the hydrogel materials are greatly affected by the hydrogel network structure and crosslinking density. Therefore, it is important to establish a relationship between the mechanical properties and network structure of hydrogels. To investigate these phenomena, we performed tensile-elongation tests on hydrogel sensors with different HEC concentrations, and their stress-strain curves are shown in Fig. 3a. The mechanical strength of the designed hydrogel increased with the increase in HEC concentration. However, beyond a certain limit there was a decrease in the mechanical strength with the increase in HEC content due to the formation of the brittle and more dense crosslinked network. The variation in strength, such as fracture stress, fracture strain, and fracture toughness is summarized in Fig. 3b, c & d, respectively. Hydrogels with 2% HEC concentration showed fracture stress of 0.34 MPa with a fracture strain of 880% and fracture energy of 1.32 MJm^{-3}. Increasing the HEC content to 3% increased the tensile stress of 0.38 MPa with a fracture strain of 1100% and a fracture energy of 1.95 MJm^{-3}. Hydrogels with 4% HEC concentration exhibited maximal tensile stress (0.51 MPa), elongation strain (1250%), and fracture energy (2.99 MJm^{-3}), and a further increase in HEC content results in a decrease in the mechanical strength (0.45 MPa stress, 1010% strain & 2.12 MJm^{-3}). Thus, we choose 4% HEC concentration as an optimum concentration for further fabrication. The

increase in tensile strength influenced by the increase in HEC content was due to a suitable number of dynamic crosslinking points, causing the formation of a compact crosslinked hydrogel network. Excess HEC content raises the viscosity of polymer solution, impeding macromolecular chain movement and free radical diffusion during the polymerization process. Thus, the creation of an unstable hydrogel network reduces the tensile strength of the engineered hydrogel.

Further, we have also investigated the PVA concentration effect on the mechanical properties of the hydrogel sensors systematically. We used three different PVA concentrations (5%, 10%, and 15%), and the stress-strain mechanical strength results are shown in Fig. 4a. The mechanical properties of the hydrogel could be tuned easily by changing the PVA concentration. At low PVA (5%) content, the hydrogel shows more stretchable, elastic, and flexible properties. The relative fracture stress, fracture strain, and fracture energy to their corresponding PVA percent concentration are given in Fig. 4b, c & d, respectively. At a low percent concentration of PVA, the hydrogel exhibited the lowest tensile stress (0.43 MPa), largest tensile strain (1350%), and moderately fracture energy (2.56 MJm^{-3}). By increasing the PVA concentration from 5 to 10%, the tensile stress reached 0.51 MPa, while there was a decrease in the elongation strain (1250%) and the highest fracture energy (2.99 MJm^{-3}). When the PVA concentration was increased to 15%, there was a decrease in fracture strain (0.42 MPa), fracture strain (1040%), and fracture energy (2.28 MJm^{-3}). These results indicate that the PVA polymer serves as a crystallite as a physical cross linker and could make more inter-and intra-hydrogen bonding interactions, which in turn improve the tensile strength of the hydrogels. These physical cross linkers could also act as energy dissipation bonds. However, the excess crosslinking will decrease the tractability and flexibility of the hydrogel network due to the formation of a brittle network. Thus, 10% PVA concentration was chosen as an optimum concentration for the fabrication of an optimized hydrogel sensor.

Incorporation of metal ions also acts as a physical crosslinking point, which produces high strength hydrogels with excellent self-healing ability due to the dissociation and association of metal-ligand bonding interaction. Therefore, we further investigate the key role of ferric ion (Fe^{3+}) concentration on the mechanical strength of the prepared hydrogel sensors. We used six different (0.05, 0.10, 0.20. 0.40, 0.60 & 0.80 M) molar concentrations of iron (III) ions for the synthesis of the hydrogel sensor. Beyond a certain limit (0.40 M), the formation of hydrogels did not take place and the four samples with 0.05––0.4 molar concentrations of iron (III) ions were subjected to tensile stress-strain tests to find their comparative mechanical strength as shown in Fig. 5a. As depicted in Fig. 5b, the tensile fracture stress increases as a function of an increase in F^{3+} ions molar concentration from 0.05 to 0.2 M and it showed the highest fracture stress (0.51 MPa) at 0.20 M concentration while further increase in metal ions content results in a decrease in tensile stress (0.40 MPa) at 0.4 M concentration. There was a dramatic change in the tensile fracture strain as a function of various metal ions concentrations. It can be seen from Fig. 5c, that at low Fe^{3+} ions concentration (0.05 & 0.10 M), the hydrogel showed higher elongation strain of 1290 & 1350%, respectively. These results indicate that a flexible, stretchable, and elastic hydrogel could be formed at low iron (III) concentration. However, at 0.20 M, the hydrogel showed the maximum tensile fracture stress (0.51 MPa), and a further increase in ferric ion content showed a decrease in both tensile

fracture stress, strain, and toughness. The trends in toughness as a function of ferric ions concentration follow the same trends as in tensile trends, which are depicted in Fig. 5d. The metal ions (Fe^{3+}) serve as physical connection points for building hydrogels with a high mechanical strength, forming coordinated bonds with PAA and HEC ligands. These bonds will dissociate and reassemble quickly and reversibly to dissipate energy and contribute to the enhancement of the hydrogels' characteristics and gradual recovery of the hydrogels' mechanical properties. The drastic shift in mechanical strength versus ferric ion content may be due to a particular phenomenon, such as the formation of mono-, di-or tridentate coordination's or retardation of radical polymerization.

The ionic coordination among the ferric ions and functional groups of ligands also affects the strength of the hydrogel network. At very low iron (III) concentration, usually bidentate (even monodentate) coordination is formed, causing lower crosslinking density in the hydrogel network, which results in worse mechanical properties. At moderate ferric ion concentration, the formation of tridentate coordination occurs, which increases the tensile stress and results in shrinkage of the hydrogel network that decreases the tensile strain of the hydrogels. Therefore, 0.20 M Fe^{3+} concentration was chosen as an appropriate concentration, which forms a considerable secondary cross-linking degree and strengthens the hydrogel materials. Additionally, the excess content of ferric ions may impede the radical polymerization of AA, causing a decrease in molecular weight of PAA polymer, which in turn lowers the mechanical strength of the designed hydrogels. We compared the mechanical properties of hydrogels to investigate the effect of the HEC, PVA, and iron (III) ions on the performance of the hydrogels. The compressive strength, tensile strength, and fracture energy of the HEC_4PVA_{10}/PAA_3-$Fe^{3+}{}_{0.2}$ hydrogels show the best performance in all samples.

Self-healing efficiency

The self-healing ability of materials not only prolongs their lifetime but also retains the materials' original properties. Autonomously self-healing in hydrogel at room temperature and without the mediation of a peripheral stimulus broadens their applications. The prepared hydrogel sensors exhibited an excellent self-healing capability, which was studied macroscopically and measured the tensile strength of healed hydrogel sensors by using (CMT4501) universal tensile testing machine. The comparative self-healing study was carried out as a function of the hydrogel composition to find their self-healing abilities and quantify the self-healing efficiencies (SHE) as a proportion of the tensile strength (TS) of the healed hydrogel to the TS of the original sample. We have also investigated the comparative percent growth ratios as a function of change in various constituents of the hydrogel sensors in original and healed samples, as summarized in Table S2. For tensile testing, the rectangular hydrogel samples were cut with a blade in the middle and rejoined the cut pieces at the cut interfaces without any external intervention. The hydrogel sensors were heald for 24 h at room temperature, before being subjected to a tensile stress-strain test to determine their mechanical healing strength. The tensile stress-strain graphs of original and healed hydrogel sensors with different HEC concentrations (2, 3, 4, & 5%) are shown in Fig. 6a. It was found that HEC concentration not only affects the mechanical strength of the hydrogels but also affects their self-healing efficiency. The trend of first increase and then decrease in stress, strain, and toughness

was also found in SHE of hydrogel sensors with different HEC concentrations as depicted in Fig. 6b. The hydrogel with 2% HEC concentration showed about 89% self-healing efficiency (SHE) in stress and with 4% HEC content SHE reached 97%. Similarly, the SHE in a strain of hydrogel sensor with HEC (2%) was 95%, which increased with the increase in HEC concentration (4%) and achieved 99% recovery in tensile strain. The recovery in toughness with 2 & 4% HEC concentration hydrogels was 83% & 94%, respectively. Further increase in HEC content results in a lower SHE in stress (85%), strain (92%), and toughness (76%).

Furthermore, we also quantified the SHE as a function of PVA concentration as shown in Fig. 6c & 6d. The hydroxyl moieties in the PVA chain play a key role in the self-healing process of hydrogel materials. At moderate concentration, PVA also shows the excellent self-recovery ability of hydrogels. The hydrogel with 5% PVA concentration got recovery of 86% in stress, 96% in strain, and 84% in toughness. On doubling the PVA concentration (PVA 10%), the SHE in stress, strain, and toughness was reached to 97%, 99%, and 94% respectively, which could be considered as an excellent recovery in hydrogel materials. A further 5% increase in PVA concentration caused a decrease in the self-healing efficiency as a whole, which may be attributed to the difficult rearrangement of hydroxyl moieties to form inter-and intrachain hydrogen bonds.

The influence of key factor Fe^{3+} ions were also studied systematically on the SHE of the hydrogel sensor and the tensile stress-strain curves of original and healed hydrogels with different Fe^{3+} ions molar concentrations are shown in Fig. 6e. All the curves of healed hydrogel obey the order of their respective original hydrogel to confirm their recovery and mechanical strength. The self-healing efficiency in stress, strain, and toughness as a function of various concentrations of iron (III) ions is shown in Fig. 6f. The trend of first increase and then decrease was also found in SHE as a function of metal ions concentration. The hydrogel containing 0.05 M Fe^{3+} ions concentration achieved about 90% recovery in stress, 93% in strain, and 83% in toughness. On increasing the concentration of metal ions from 0.05 M to 0.20 M, the SHE in stress, strain, and toughness reached 97%, 99%, and 93%, respectively. Further increase in the metal ions concentration causes a decrease in SHE in stress, strain, and toughness to 90%, 93%, and 83%, respectively. The mobilized Fe^{3+} ions and polymers chain plays a critical role in the process of self-healing, which diffuse towards the cut interfaces and interact with the functional groups of polymer chain to re-establish the ionic coordination. However, at higher Fe^{3+} ions concentration, a rigid hydrogel network is formed that hinders the free diffusion of metal ions and polymer chain, and therefore the self-healing ability of the hydrogel gradually decreases.

The mechanical healing efficiency was also studied as a function of healing time on the optimized hydrogel sensors. The two freshly cut pieces were healed for different time intervals (3, 6, 12 & 24 h) without any external intervention at room temperature. The healed specimen was subjected to the stress-strain tests and their relative was compared strength with the original hydrogel sample, as shown in Fig. 7a. Hydrogel recovered 73% in stress, 84% in strain, and 60% in toughness, even at the shortest healing time of 3 hours. With an increasing in healing time, the self-healing efficiency also increases and achieved 91% SHE in strain, 99% SHE in strain, and 94% SHE in toughness after a healing time of 24 h, as

represented in Fig. 7b. The comparative fracture stress, strain, and toughness of original and healed hydrogel sensors as a function of the healing time are depicted in Fig. 7c.

The self-healing ability was also studied macroscopically as shown in Fig. 8. The freshly prepared hydrogel was cut into small pieces with a sharp cutter. The cut pieces were placed together in a self-made dumbbell-shaped mold, pressed between two glass plates, and were healed at room temperature for 24 h, as shown in Fig. 8a. It was interesting to find that the cut pieces were healed together and formed a desired shaped hydrogel without any visible fracture and scratch (Fig. 8b). The healed hydrogel showed strong mechanical strength that can be bent and twist without any fracture (Fig. 8c). Thus, we can say that the designed hydrogel has excellent self-healing ability.

The supreme self-healing capability of the hydrogel sensor is due to two types of interactions, i.e. ionic and hydrogen bonding interactions. The hydroxyl moieties in the poly (vinyl alcohol) (PVA) chain form hydrogen bonding with the adjacent chains on the contact of two cut pieces. The polymer chains diffuse transversely through the interface and the reformation of the new hydrogen bonding occurs. However, the rearrangement of the hydroxyl moieties in the PVA hydrogel to reform intra and inter-chain hydrogen bonds limits the predominant self-healing ability of PVA hydrogels. The self-healing of hydrogel sensor is endorsed by the natural transmission of PVA; HEC; and PAA polymer chains, ferric ions and water at the cut edges, and the successive formation of hydrogen bonding. The simultaneous diffusion and subsequent entanglement of Fe^{3+} ions and PAA chain across the cut interfaces help in the self-healing ability of hydrogel due to the Fe^{3+} ions mediated ionic interaction and hydrogen bonding association.

Electrochemical and sensing performance

Electrochemical impedance spectroscopy was used to measure the ionic conductivity of the hydrogel sensor and its Nyquist plot is represented in Fig. 9a. The initial semicircular pattern of the Nyquist plot indicates the charge transfer and then the linear curve shows the mass transfer electrical conductivity. The starting point observed at the start of the high frequency is the electrolyte resistance (R_s) and the charge-transfer resistance (R_p) can be determined by the diameter of the semicircle. The hydrogel showed about 2.22×10^{-1} S m^{-1} electrical conductivity at room temperature, which is sufficient for use in the fabrication of biomedical e-skins, soft robotics, health monitoring, and biomedical diagnostic devices. The mobile ferric ions and free electrons on carboxylate ions in the hydrogel network greatly contributed to the electrical conductivity of hydrogels. To investigate the probability of the hydrogel as a strain sensor, the hydrogels were subjected to relative electrical resistance change tests as a function of assorted strain. The sensitivity of the strain sensor was measured by finding their linearity as a change in the relative electrical signals as a function of applied strain (%), as depicted in Fig. 9b. The relative change in resistance ($\Delta R/R_0$ (%) increases linearly with an increase in strain from 0 to 400% and reached to 340%, indicating superior sensitivity of the prepared hydrogel sensor. The stability of the sensor was measured by holding-loading a stepwise test as a change in $\Delta R/R_0$ (%) versus time (s) and sustained for a while at some specific strain. The hydrogel exhibited steps of stair-like trends as displayed in Fig. 9c, in which the $\Delta R/R_0$ (%) shows direct proportion with the change in strain (%) and maintains a specific strain for some

time without any change in the (ΔR/R (%), indicating outstanding stability in resistance as a function of various stains. The reliability and durability of the hydrogel sensor were further investigated through the electromechanical (EM) cyclic test as a relative change in resistance as a function of time (s) and the results are depicted in Fig. 9d. The EM loading-unloading signals in Fig. 9d almost show similar trends in their resistance change versus time, which confirm their excellent durability and reliability in EM behavior. These results indicate that the designed hydrogel sensor is a stable, sensitive, reliable, and durable sensor, which can boost its long life expectancy.

To investigate the performance of hydrogel as a wearable strain sensor in a real-time application, the pressure-based strain sensors were directly attached to the numerous junction points (index finger and wrist joints) of a human body for monitoring various human motions. The relative change in resistance at various strains was measured by monitoring the movements of these muscular joints.

The sensitivity, ionic conductivity, and feasibility of the hydrogel-based sensor were recorded *via* a bending-holding process by bending the index finger and holding for some time at fixed strain, as shown in Fig. 10a. The hydrogel demonstrated a relative change in resistance as a function of time with an increase in finger bending angle as a steps of stair trend. Bending the finger causes the hydrogel to stretch, which increases the relative resistance, and at a constant angle, the ΔR/R (%) remains constant, indicating accurate control of the finger moment. Several consecutive electromechanical loading-unloading cycles were used for the analysis of the reliability of electrical conductance on the bending figure as shown in Fig. 10b. The cyclical bending of the hydrogel sensor on the forefinger produced nearly identical signals, indicating that the sensor's responsive activity is repeatable and consistent.

The hydrogel sensor was further subjected to 100 cycles at 50% strain in the EM loading-unloading test and the results are displayed in Fig. 10c. The cyclic EM loading-unloading curves (inset Fig. 10C) showed almost identical intensity at a 50% strain, indicating their stability and long lifespan as a strain sensor. This was further confirmed by a cyclic bending-relaxing test of the wrist joints and a stable ΔR/R (%) as a function of time was obtained as displayed in Fig. 10d that further confirms their durability, stability, and recoverability. Based on this performance, the prepared hydrogel has the potential for e-skin applications that could be used as a wearable strain sensor to monitor and quantify various human motions in real-time.

Conclusion

In summary, we have designed a self-healing hydrogel strain sensor that can be used to sense various human motions. The designed hydrogel possesses high mechanical stress (0.51 MPa), excellent stretchability (1250%), outstanding self-healing efficiency (98%), and good conductivity (2.21×10^{-1} Sm^{-1}). The addition of HEC significantly enhanced the mechanical strength and healing efficiencies at room temperature without using any external healing agent. The healing was driven by the re-association of

hydrogen and ionic interaction between the cut surfaces of the hydrogel. Controlling the crosslinking density of various constitutes in the hydrogel network allows for tuning of mechanical properties and healing efficiency. The self-healing of the hydrogel sensor potentially enhances their functional lifespan. The tunneling effect imparts high sensitivity, stability, durability, and broad detection range to the hydrogel strain sensors and enables them to monitor a wide range of human motion at room temperature. Considering the stability, high sensitivity, durability, and repeatability of the signals during the detection of various human motion, this self-healable and ultra-stretchable strain sensor has potential applications in various fields, including sports, robotics, bio-sensors, electronic skin health monitoring, etc. Briefly, this work offers a novel strategy for the development of high strength and self-healable conductive hydrogel sensors that can be used as functional self-healing electrochemical sensor devices, such as artificial soft actuators, solar cells, semiconductors, and wearable sensors.

Declarations

Acknowledgments

This work was supported by the Nanjing Forestry University “Metasequoia talent research start-up fund (Project No.163101071).

References

1. Amoli V, Kim JS, Jee E, Chung YS, Kim SY, Koo J, Choi H, Kim Y, Kim DHJNc (2019) A bioinspired hydrogen bond-triggered ultrasensitive ionic mechanoreceptor skin. Nature Communications 10 (1):1-13
2. Calvert PJAm (2009) Hydrogels for soft machines. Adv Mater 21 (7):743-756. https://doi.org/10.1038/s41467-019-11973-5
3. Cao Y, Morrissey TG, Acome E, Allec SI, Wong BM, Keplinger C, Wang CJAM (2017) A transparent, self-healing, highly stretchable ionic conductor. Adv Mater 29 (10):1605099. https://doi.org/10.1002/adma.201605099
4. Chen J, Yu Q, Cui X, Dong M, Zhang J, Wang C, Fan J, Zhu Y, Guo ZJJoMCC (2019) An overview of stretchable strain sensors from conductive polymer nanocomposites. Journal of materials Chemistry C 7 (38):11710-11730. https://doi.org/10.1039/C9TC03655E
5. Depalle B, Qin Z, Shefelbine SJ, Buehler MJJJotmbobm (2015) Influence of cross-link structure, density and mechanical properties in the mesoscale deformation mechanisms of collagen fibrils. Journal of the Mechanical Behavior of Biomedical Materials 52:1-13. https://doi.org/10.1016/j.jmbbm.2014.07.008
6. Feig VR, Tran H, Lee M, Bao ZJNc (2018) Mechanically tunable conductive interpenetrating network hydrogels that mimic the elastic moduli of biological tissue. Nat Commun 9 (1):1-9. DOI: 10.1038/s41467-018-05222-4

7. Gong JP, Katsuyama Y, Kurokawa T, Osada YJAm (2003) Double-network hydrogels with extremely high mechanical strength. Adv Mater 15 (14):1155-1158. https://doi.org/10.1002/adma.200304907
8. Guo S, Wen D, Zhai Y, Dong S, Wang EJAn (2010) Platinum nanoparticle ensemble-on-graphene hybrid nanosheet: one-pot, rapid synthesis, and used as new electrode material for electrochemical sensing. ACS Nano 4 (7):3959-3968. *DOI:* 10.1021/nn100852h
9. Hao X, Liu H, Lu Z, Xie Y, Yang HJJoMCA (2013) Endowing the conventional HMPAM hydrogel with pH-responsive and self-healing properties. J Mater Chem A 1 (23):6920-6927. https://doi.org/10.1039/C3TA10285H
10. He H, Zhang L, Guan X, Cheng H, Liu X, Yu S, Wei J, Ouyang JJAam, interfaces (2019) Biocompatible conductive polymers with high conductivity and high stretchability.
11. ACS Appl Mater Interfaces 11 (29):26185-26193. DOI: 10.1021/acsami.9b07325
12. Huang T, Xu H, Jiao K, Zhu L, Brown HR, Wang HJAM (2007) A novel hydrogel with high mechanical strength: a macromolecular microsphere composite hydrogel. Adv Mater 19 (12):1622-1626. https://doi.org/10.1002/adma.200602533
13. Kakuta T, Takashima Y, Nakahata M, Otsubo M, Yamaguchi H, Harada AJAm (2013) Preorganized hydrogel: self-healing properties of supramolecular hydrogels formed by polymerization of host–guest-monomers that contain cyclodextrins and hydrophobic guest groups. Adv Mater 25 (20):2849-2853. https://doi.org/10.1002/adma.201205321
14. Kean ZS, Hawk JL, Lin S, Zhao X, Sijbesma RP, Craig SLJAM (2014) Increasing the maximum achievable strain of a covalent polymer gel through the addition of mechanically invisible cross-links. Adv Mater 26 (34):6013-6018. https://doi.org/10.1002/adma.201401570
15. Kim J, Lee G, Heimgartner R, Revi DA, Karavas N, Nathanson D, Galiana I, Eckert-Erdheim A, Murphy P, Perry DJS (2019) Reducing the metabolic rate of walking and running with a versatile, portable exosuit. Science 365 (6454):668-672. DOI: 10.1126/science.aav7536
16. Kushner AM, Gabuchian V, Johnson EG, Guan ZJJotACS (2007) Biomimetic design of reversibly unfolding cross-linker to enhance mechanical properties of 3D network polymers. journal of American Chemical Society 129 (46):14110-14111. https://doi: 10.1021/ja0742176
17. Lei Z, Wu PJNc (2018) A supramolecular biomimetic skin combining a wide spectrum of mechanical properties and multiple sensory capabilities. Nat Commun 9 (1):1-7. https://doi.org/10.1038/s41467-018-03456-w
18. Li S, Qin H, Zhang T, Cong HP, Yu SHJS (2018) Highly Tough Bioinspired Ternary Hydrogels Synergistically Reinforced by Graphene/Xonotlite Network. Small 14 (22):1800673. https://doi.org/10.1002/smll.201800673
19. Liao M, Wan P, Wen J, Gong M, Wu X, Wang Y, Shi R, Zhang LJAFM (2017) Wearable, healable, and adhesive epidermal sensors assembled from mussel-inspired conductive hybrid hydrogel framework. Advanced Functional Materials 27 (48):1703852. https://doi.org/10.1002/adfm.201703852
20. Lin P, Ma S, Wang X, Zhou FJAM (2015) Molecularly engineered dual-crosslinked hydrogel with ultrahigh mechanical strength, toughness, and good self-recovery. Adv Mater 27 (12):2054-2059.

https://doi.org/10.1002/adma.201405022

21. Lipomi DJ, Vosgueritchian M, Tee BC, Hellstrom SL, Lee JA, Fox CH, Bao ZJNn (2011) Skin-like pressure and strain sensors based on transparent elastic films of carbon nanotubes. Nature Nanotechnology 6 (12):788-792. https://doi.org/10.1038/nnano.2011.184
22. Odent J, Wallin TJ, Pan W, Kruemplestaedter K, Shepherd RF, Giannelis EPJAFM (2017) Highly elastic, transparent, and conductive 3D-printed ionic composite hydrogels. Advanced Functional Materials 27 (33):1701807. https://doi.org/10.1002/adfm.201701807
23. Okumura Y, Ito KJAm (2001) The polyrotaxane gel: A topological gel by figure-of-eight cross-links. Adv Mater 13 (7):485-487. https://doi.org/10.1002/1521-4095(200104)13:7<485::AID-ADMA485>3.0.CO;2-T
24. Pang C, Lee G-Y, Kim T-i, Kim SM, Kim HN, Ahn S-H, Suh K-YJNm (2012) A flexible and highly sensitive strain-gauge sensor using reversible interlocking of nanofibres. Nature Mater 11 (9):795-801. https://doi: 10.1038/nmat3380
25. Qin Z, Sun X, Zhang H, Yu Q, Wang X, He S, Yao F, Li JJJoMCA (2020) A transparent, ultrastretchable and fully recyclable gelatin organohydrogel based electronic sensor with broad operating temperature. J Mater Chem A 8 (8):4447-4456. https://doi.org/10.1039/C9TA13196E
26. Sarwar MS, Dobashi Y, Preston C, Wyss JK, Mirabbasi S, Madden JDWJSa (2017) Bend, stretch, and touch: Locating a finger on an actively deformed transparent sensor array. Science Advances 3 (3):e1602200. https://doi:10.1126/sciadv.1602200
27. Shin W-K, Cho J, Kannan AG, Lee Y-S, Kim D-WJSr (2016) Cross-linked composite gel polymer electrolyte using mesoporous methacrylate-functionalized SiO 2 nanoparticles for lithium-ion polymer batteries. Scientific Report 6 (1):1-10. https://doi: 10.1038/srep26332
28. Someya T, Sekitani T, Iba S, Kato Y, Kawaguchi H, Sakurai TJPotNAoS (2004) A large-area, flexible pressure sensor matrix with organic field-effect transistors for artificial skin applications. Proc Natl Acad Sci U S A 101 (27):9966-9970. https://doi.org/10.1073/pnas.0401918101
29. Sun TL, Kurokawa T, Kuroda S, Ihsan AB, Akasaki T, Sato K, Haque MA, Nakajima T, Gong JPJNm (2013a) Physical hydrogels composed of polyampholytes demonstrate high toughness and viscoelasticity. Nature Materials 12 (10):932-937. https://doi.org/10.1038/nmat3713
30. Tee BC, Wang C, Allen R, Bao ZJNn (2012) An electrically and mechanically self-healing composite with pressure-and flexion-sensitive properties for electronic skin applications. Nature Nanotechnology 7 (12):825-832. https://doi.org/10.1038/nnano.2012.192
31. Wan S, Fang S, Jiang L, Cheng Q, Baughman RHJAM (2018) Strong, conductive, foldable graphene sheets by sequential ionic and π bridging. Adv Mater 30 (36):1802733. https://doi.org/10.1002/adma.201802733
32. Wang J, Gao W, Zhang H, Zou M, Chen Y, Zhao YJSA (2018a) Programmable wettability on photocontrolled graphene film. Science Advances 4 (9):eaat7392. https://doi: 10.1126/sciadv.aat7392

33. Wang J, Lin L, Cheng Q, Jiang LJACIE (2012) A strong bio-inspired layered PNIPAM–clay nanocomposite hydrogel. Angewandte Chemie 51 (19):4676-4680. https://doi.org/10.1002/anie.201200267
34. Wang J, Tang F, Wang Y, Lu Q, Liu S, Li LJAam, interfaces (2019a) Self-healing and highly stretchable gelatin hydrogel for self-powered strain sensor. ACS Appl Mater Interfaces 12 (1):1558-1566. https://doi:10.1021/acsami.9b18646
35. Wang K, Lou Z, Wang L, Zhao L, Zhao S, Wang D, Han W, Jiang K, Shen GJAn (2019b) Bioinspired interlocked structure-induced high deformability for two-dimensional titanium carbide (MXene)/natural microcapsule-based flexible pressure sensors. ACS Nano 13 (8):9139-9147. https://doi: 10.1021/acsnano.9b03454
36. Wang T, Zhang Y, Liu Q, Cheng W, Wang X, Pan L, Xu B, Xu HJAFM (2018b) A self-healable, highly stretchable, and solution processable conductive polymer composite for ultrasensitive strain and pressure sensing. Advanced Functional Materials 28 (7):1705551. https://doi.org/10.1002/adfm.201705551
37. Williams KA, Boydston AJ, Bielawski CWJJotrsi (2007) Towards electrically conductive, self-healing materials. journal of the Royal Society Interface 4 (13):359-362. https://doi.org/10.1098/rsif.2006.0202
38. Xia L-W, Xie R, Ju X-J, Wang W, Chen Q, Chu L-YJNc (2013) Nano-structured smart hydrogels with rapid response and high elasticity. Nat Commun 4 (1):1-11. https://doi.org/10.1038/ncomms3226
39. Xin Y, Qi X, Tian H, Guo C, Li X, Lin J, Wang CJML (2016) Full-fiber piezoelectric sensor by straight PVDF/nanoclay nanofibers. Materials Letters 164:136-139. https://doi.org/10.1016/j.matlet.2015.09.117
40. Xu R, Ma S, Lin P, Yu B, Zhou F, Liu WJAam, interfaces (2017) High strength astringent hydrogels using protein as the building block for physically cross-linked multi-network. ACS Appl Mater Interfaces 10 (9):7593-7601. https://doi: 10.1021/acsami.7b04290
41. Xu S, Jayaraman A, Rogers JA (2019) Skin sensors are the future of health care. Nature 571(7765):319-321. https://doi:10.1038/d41586-019-02143-0
42. Yan Q, Zhou M, Fu HJCPBE (2020) Study on mussel-inspired tough TA/PANI@ CNCs nanocomposite hydrogels with superior self-healing and self-adhesive properties for strain sensors. Composites Part B: Engineering 201:108356. https://doi.org/10.1016/j.compositesb.2020.108356
43. Yu Q, Qin Z, Ji F, Chen S, Luo S, Yao M, Wu X, Liu W, Sun X, Zhang HJCEJ (2021) Low-temperature tolerant strain sensors based on triple crosslinked organohydrogels with ultrastretchability. Chemical Engineering Journal 404:126559. https://doi.org/10.1016/j.cej.2020.126559
44. Yu Y, Guo J, Sun L, Zhang X, Zhao YJR (2019) Microfluidic generation of microsprings with ionic liquid encapsulation for flexible electronics. Research 2019. https://doi.org/10.34133/2019/6906275
45. Zeng X, Wang Z, Zhang H, Yang W, Xiang L, Zhao Z, Peng L-M, Hu YJAam, interfaces (2019) Tunable, ultrasensitive, and flexible pressure sensors based on wrinkled microstructures for electronic skins. ACS Appl Mater Interfaces 11 (23):21218-21226. https://doi:10.1021/acsami.9b02518

46. Zhang H, Xia H, Zhao YJAML (2012) Poly (vinyl alcohol) hydrogel can autonomously self-heal. ACS Macro Latters 1 (11):1233-1236. https://doi.org/10.1021/mz300451r
47. Zhang Q, Liu X, Ren X, Jia F, Duan L, Gao GJCoM (2019a) Nucleotide-regulated tough and rapidly self-recoverable hydrogels for highly sensitive and durable pressure and strain sensors. Chemistry of Materials 31 (15):5881-5889. https://doi.org/10.1021/acs.chemmater.9b02039
48. Zhang X, Sheng N, Wang L, Tan Y, Liu C, Xia Y, Nie Z, Sui KJMH (2019b) Supramolecular nanofibrillar hydrogels as highly stretchable, elastic and sensitive ionic sensors. Mater Horizons 6 (2):326-333. https://doi.org/10.1039/C8MH01188E
49. Zhou Y, Wan C, Yang Y, Yang H, Wang S, Dai Z, Ji K, Jiang H, Chen X, Long YJAFM (2019) Highly stretchable, elastic, and ionic conductive hydrogel for artificial soft electronics. Advanced Functional Materials 29 (1):1806220. https://doi.org/10.1002/adfm.201806220
50. Zhu C, Chalmers E, Chen L, Wang Y, Xu BB, Li Y, Liu XJS (2019) A Nature-Inspired, Flexible Substrate Strategy for Future Wearable Electronics. Small 15 (35):1902440. https://doi.org/10.1002/smll.201902440

Figures

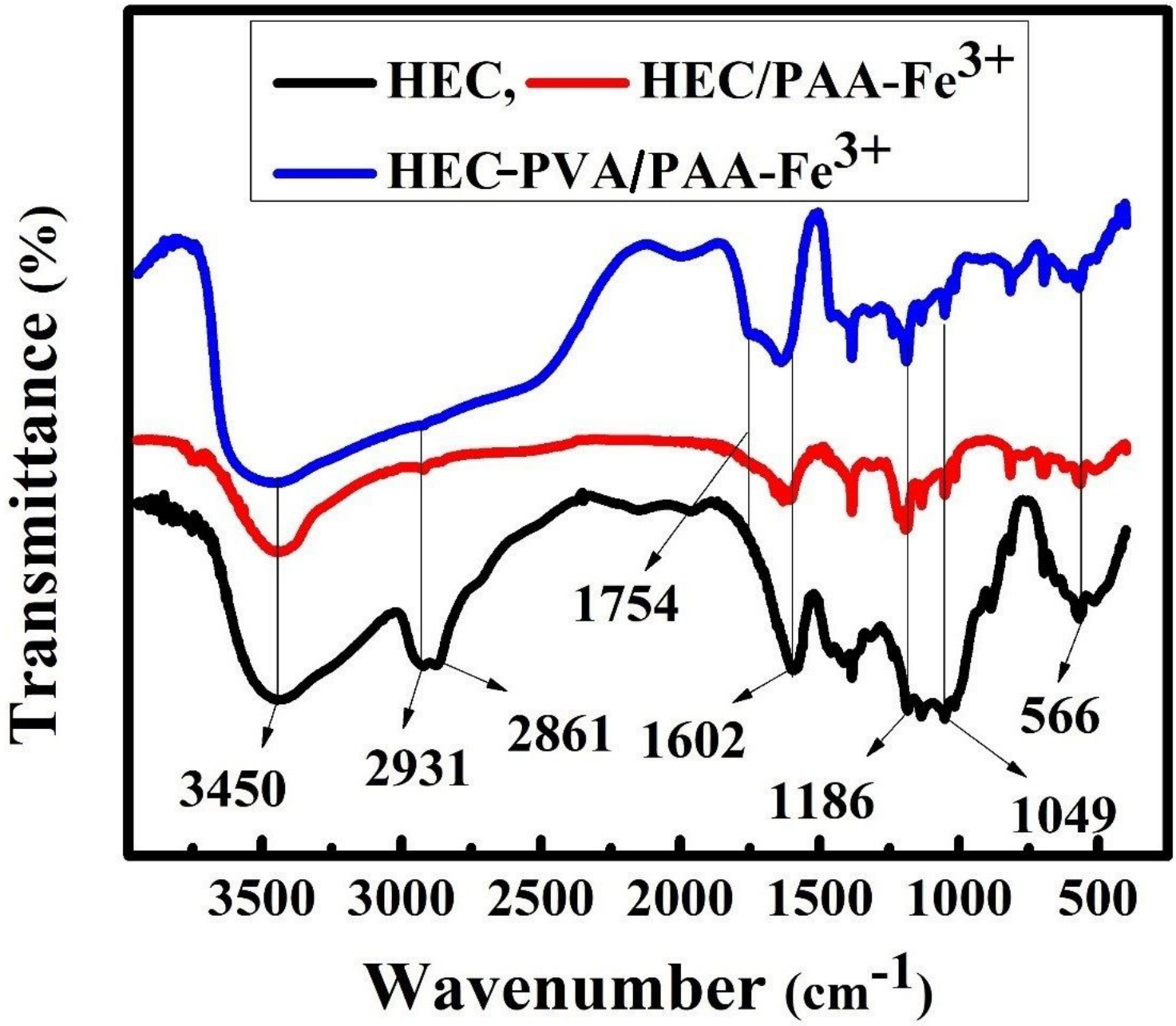

Figure 1

FTIR spectra of HEC, HEC/PAA-Fe3+ and HEC-PVA/PAA-Fe3+ Hydrogels

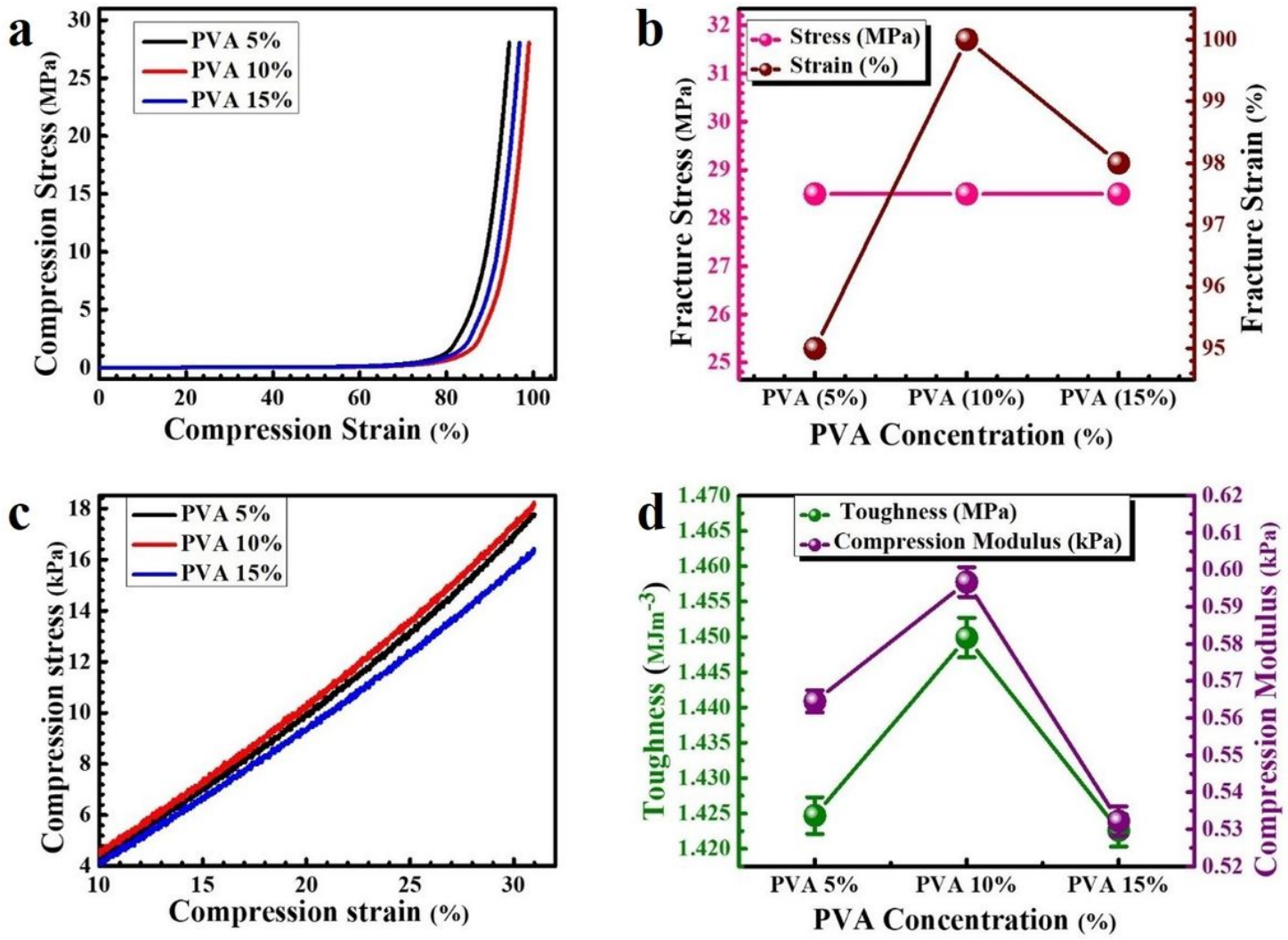

Figure 2

Graphs show the (a) Compression strength of Hydrogels with different PVA percent concentration; (b) compression fracture stress and strain; (c) Initial 10-30% compression modulus strength; and (d) toughness and compression moduli of hydrogel samples with various PVA % concentration

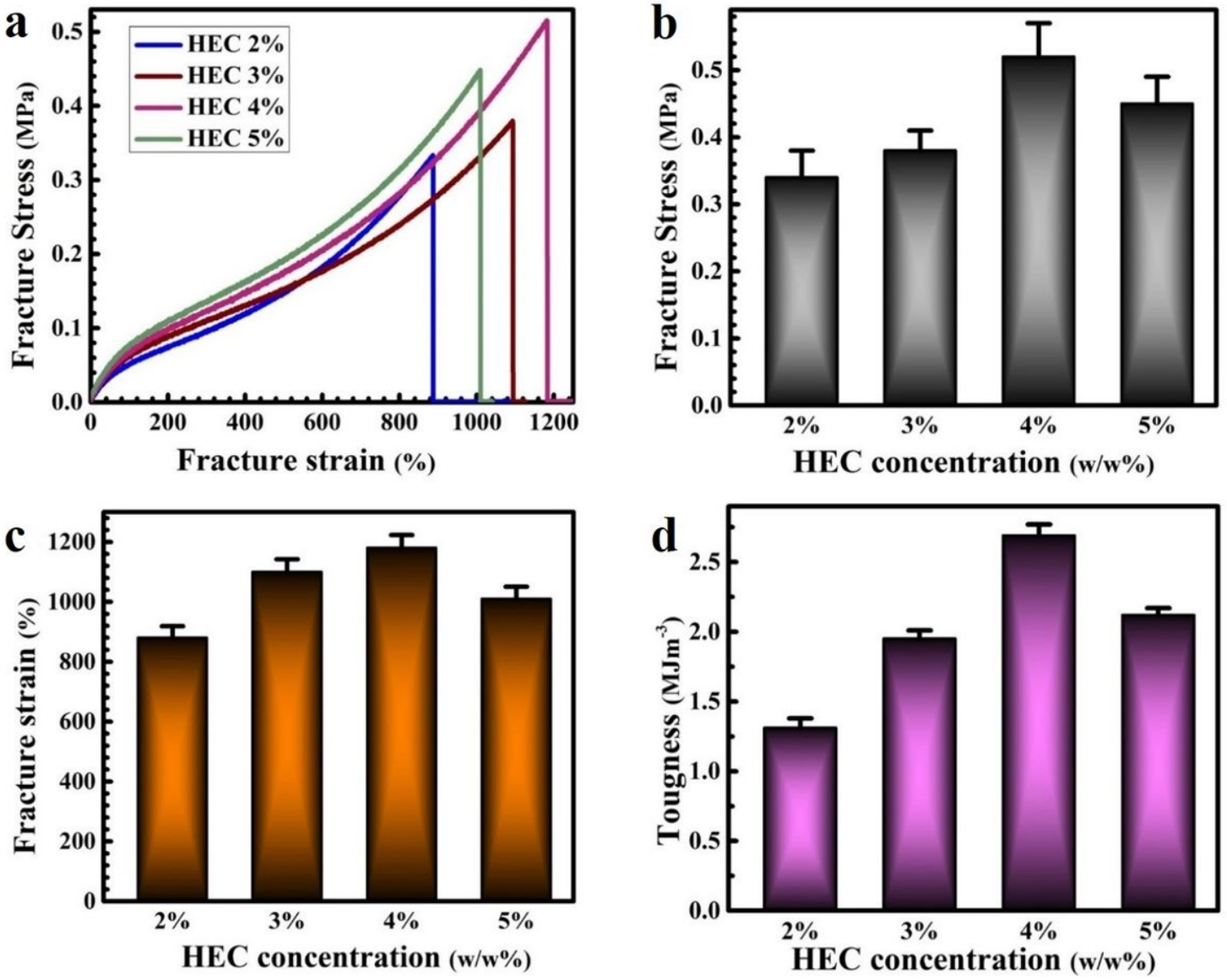

Figure 3

The graphs represent (a) the tensile stress-strain strength; (b) fracture stress; (c) fracture strain; and (d) fracture strain of hydrogel with different HEC percent concentrations

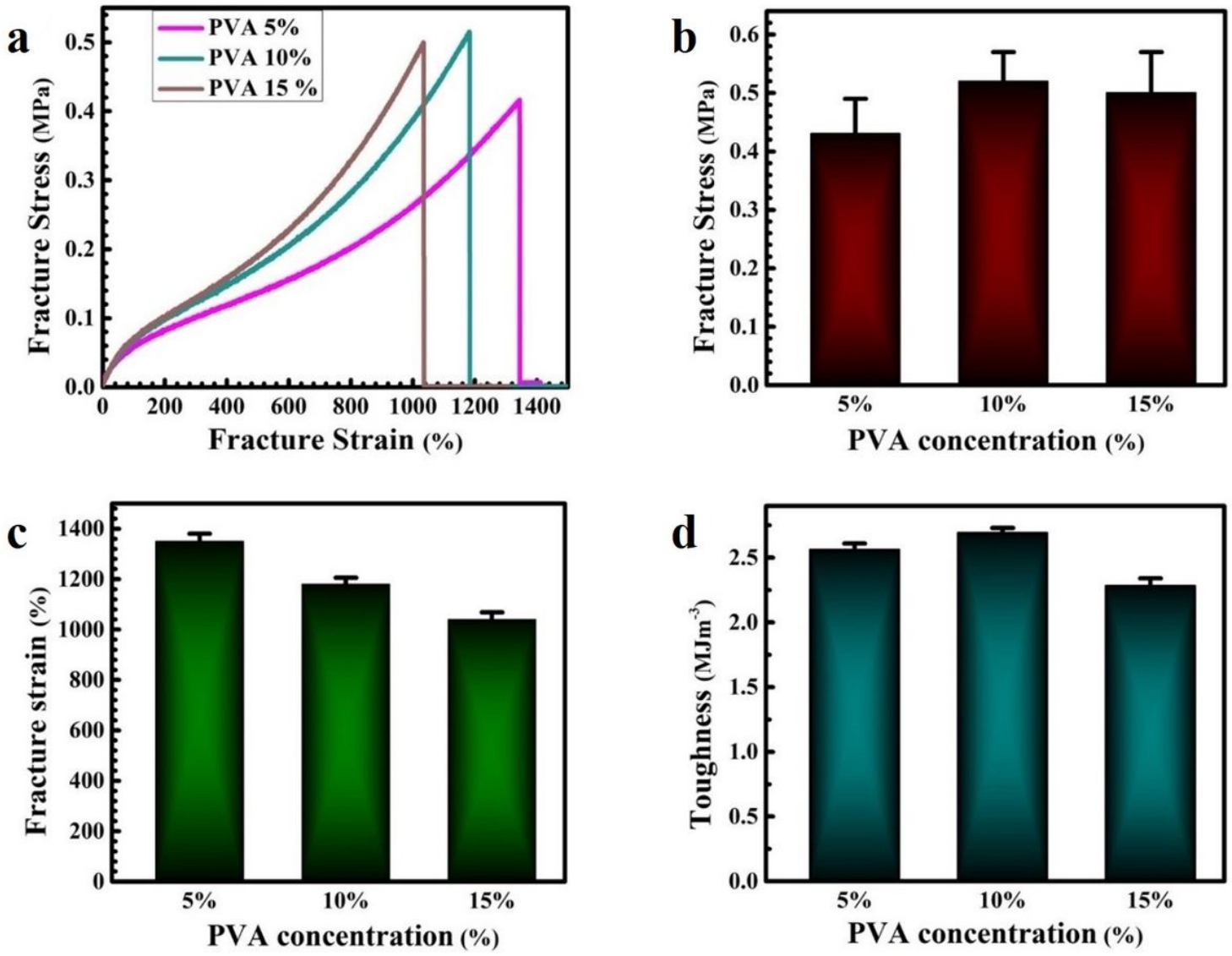

Figure 4

Graph shows (a) the tensile stress-strain strength; (b) fracture stress; (c) fracture strain; and (d) fracture toughness of hydrogel samples with different PVA percent concentrations

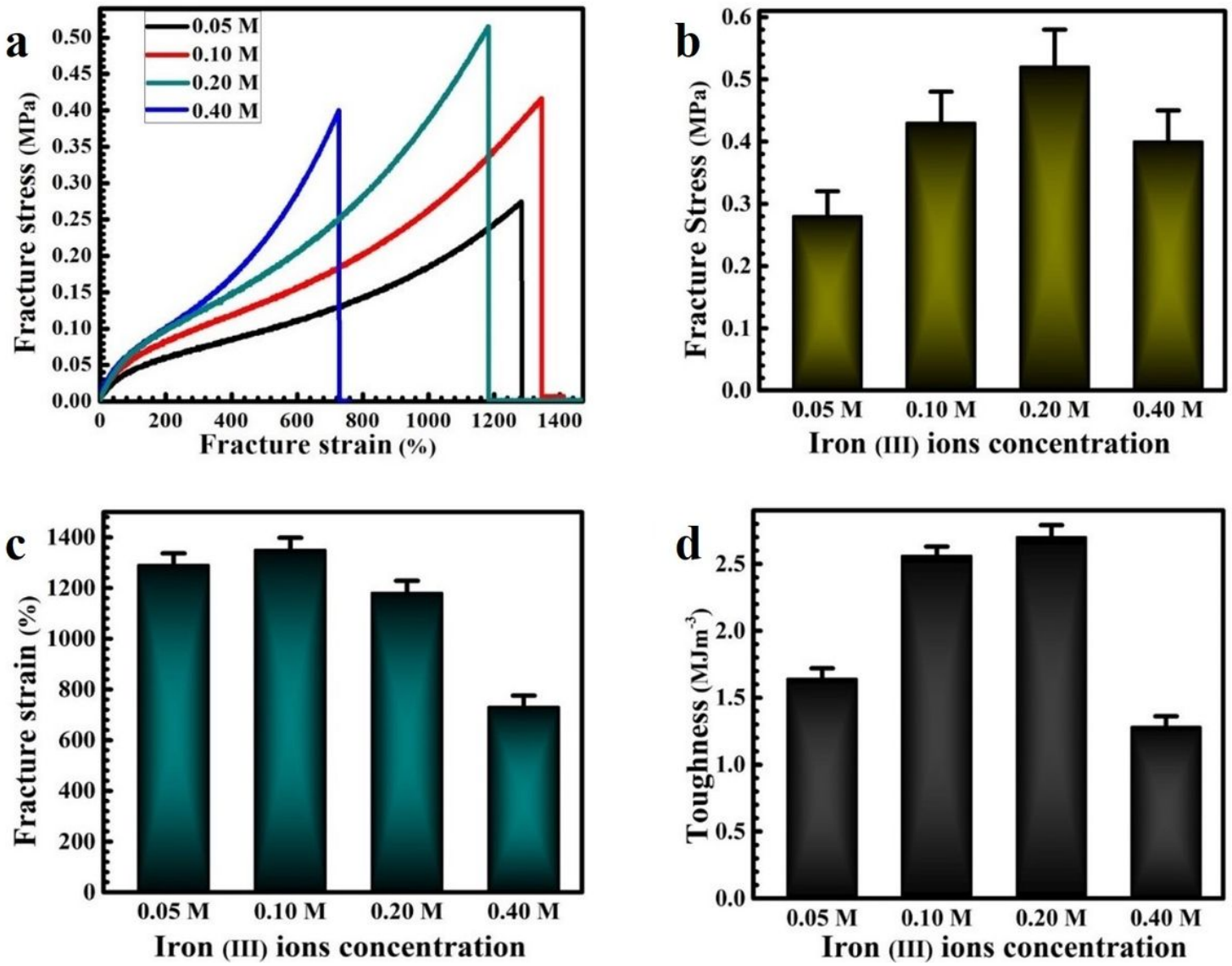

Figure 5

(a) the tensile stress-strain curves; (b) fracture tensile stress; (c) fracture tensile strain, and (d) fracture tensile toughness of hydrogel samples with various Fe3+ molar concentration

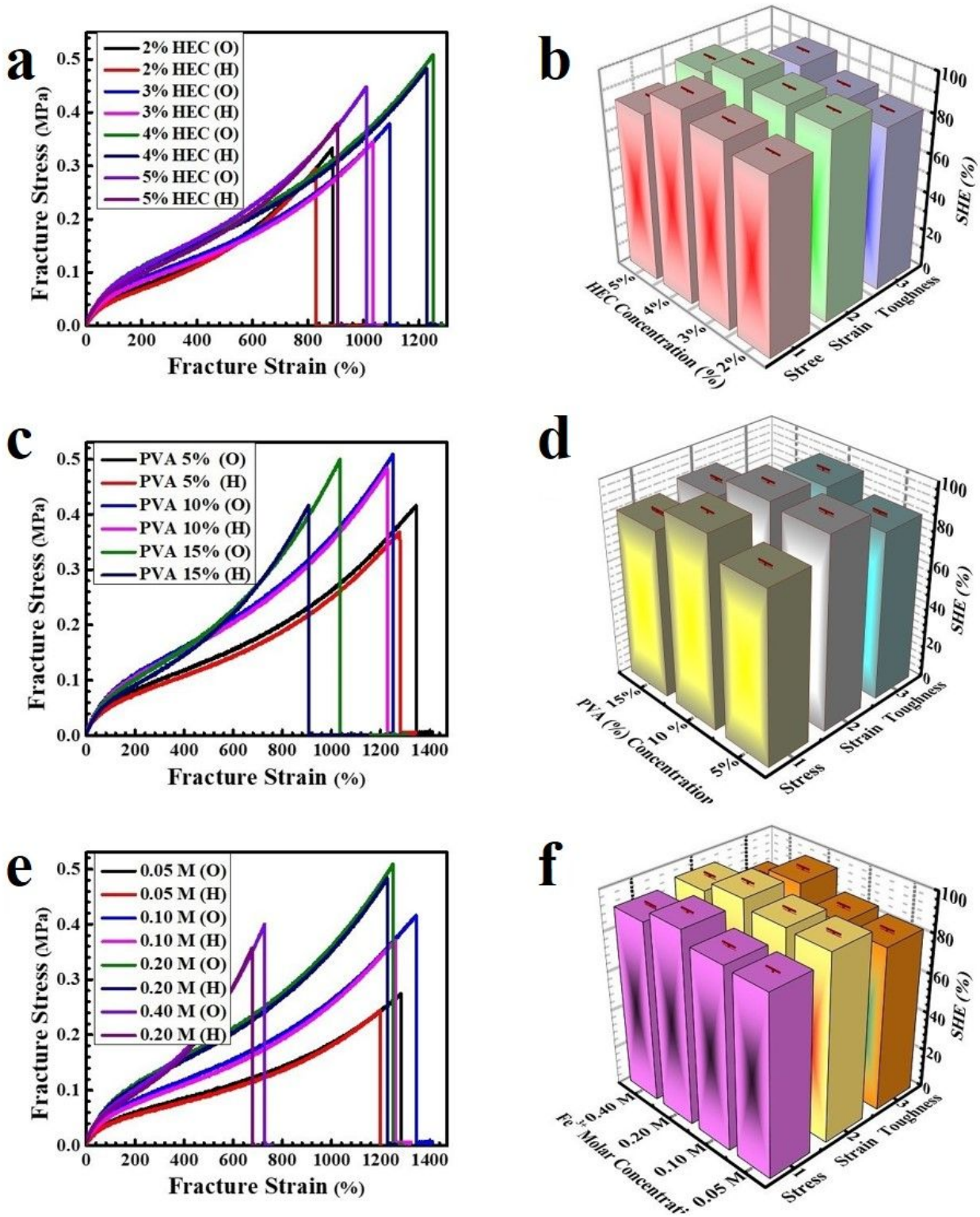

Figure 6

Graphs show (a) the self-healing ability of hydrogel with different HEC percent concentration; (b) self-healing efficiency in stress, strain & toughness with different HEC%; (c) self-healing capability with various PVA5% concentration; (d) self-healing efficiency in stress, strain & toughness with different PVA% concentration; (e) self-healing of hydrogel with various Fe3+ molar concentration; and (f) self-healing efficiency in stress, strain & toughness of hydrogel samples with different Fe3+ molar concentration

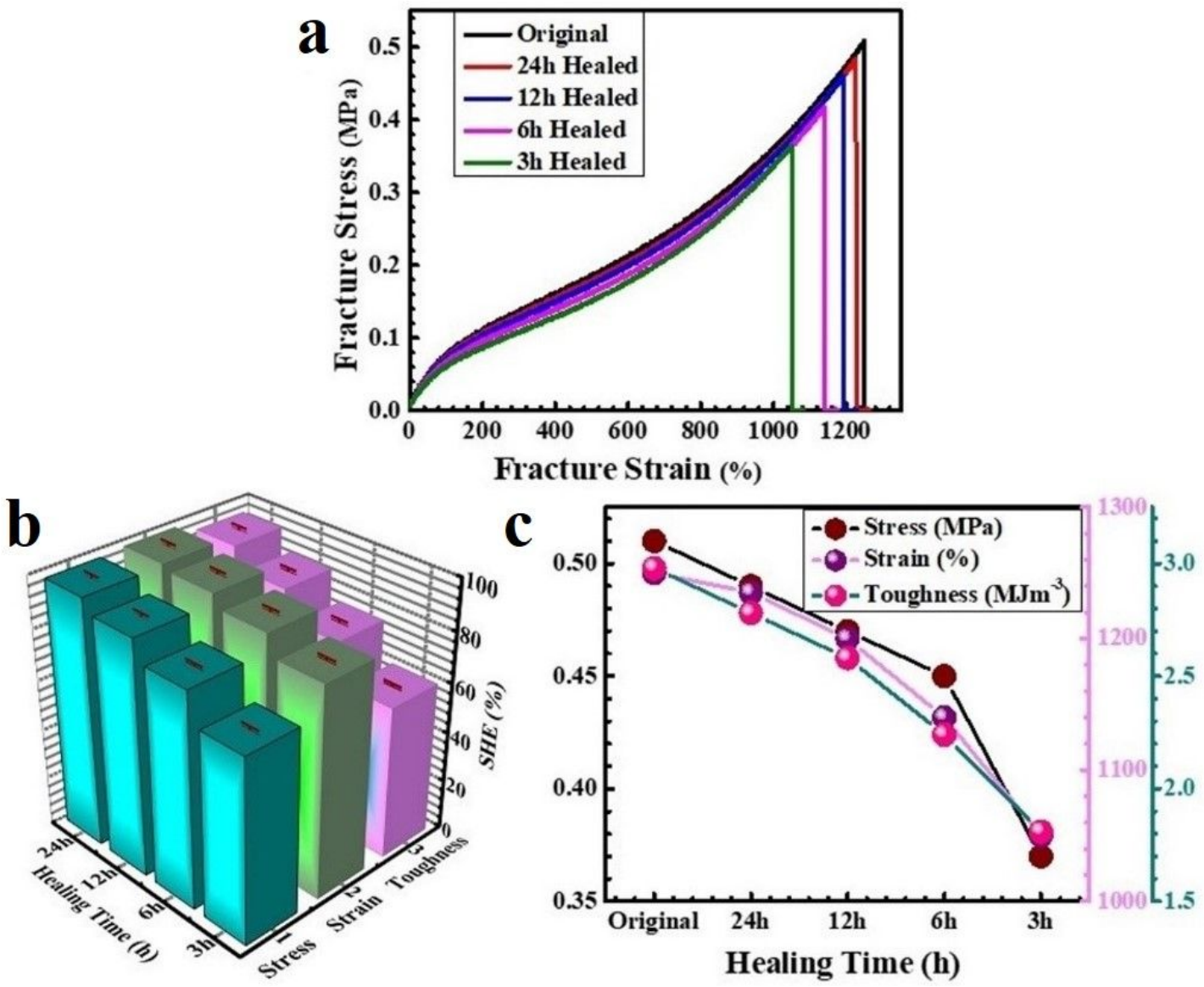

Figure 7

(a) self-healing of hydrogel healed at different time intervals; (b) self-healing efficiency in stress, strain & toughness w.r.t. time; and (c) fracture stress, strain, and toughness of original and healed hydrogel samples.

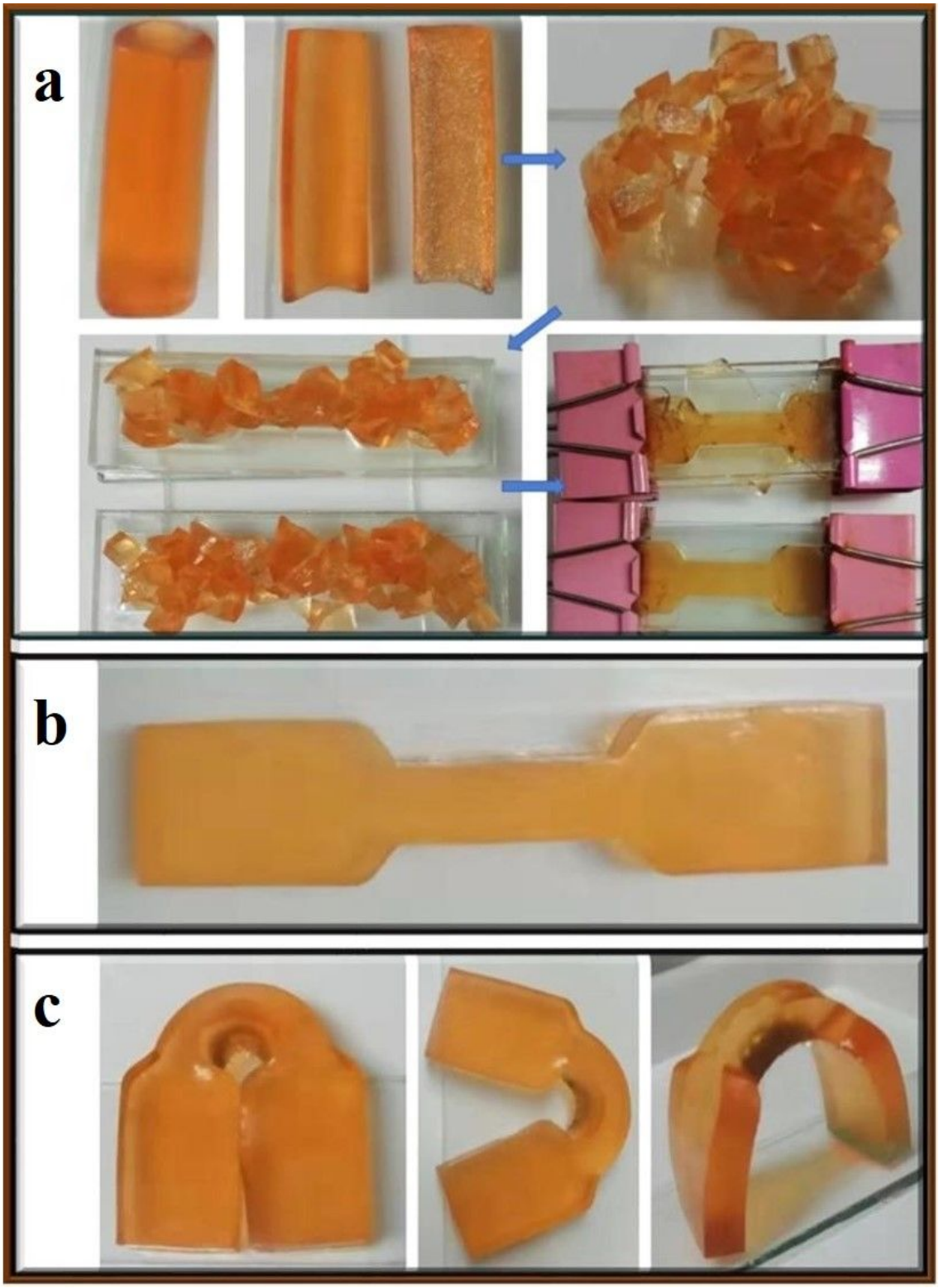

Figure 8

The digital image show (a) the original hydrogel cut into small pieces with a knife and rejoin to reform hydrogel; (b) healed hydrogel after 24 hours; (c) mechanical strength of healed hydrogel.

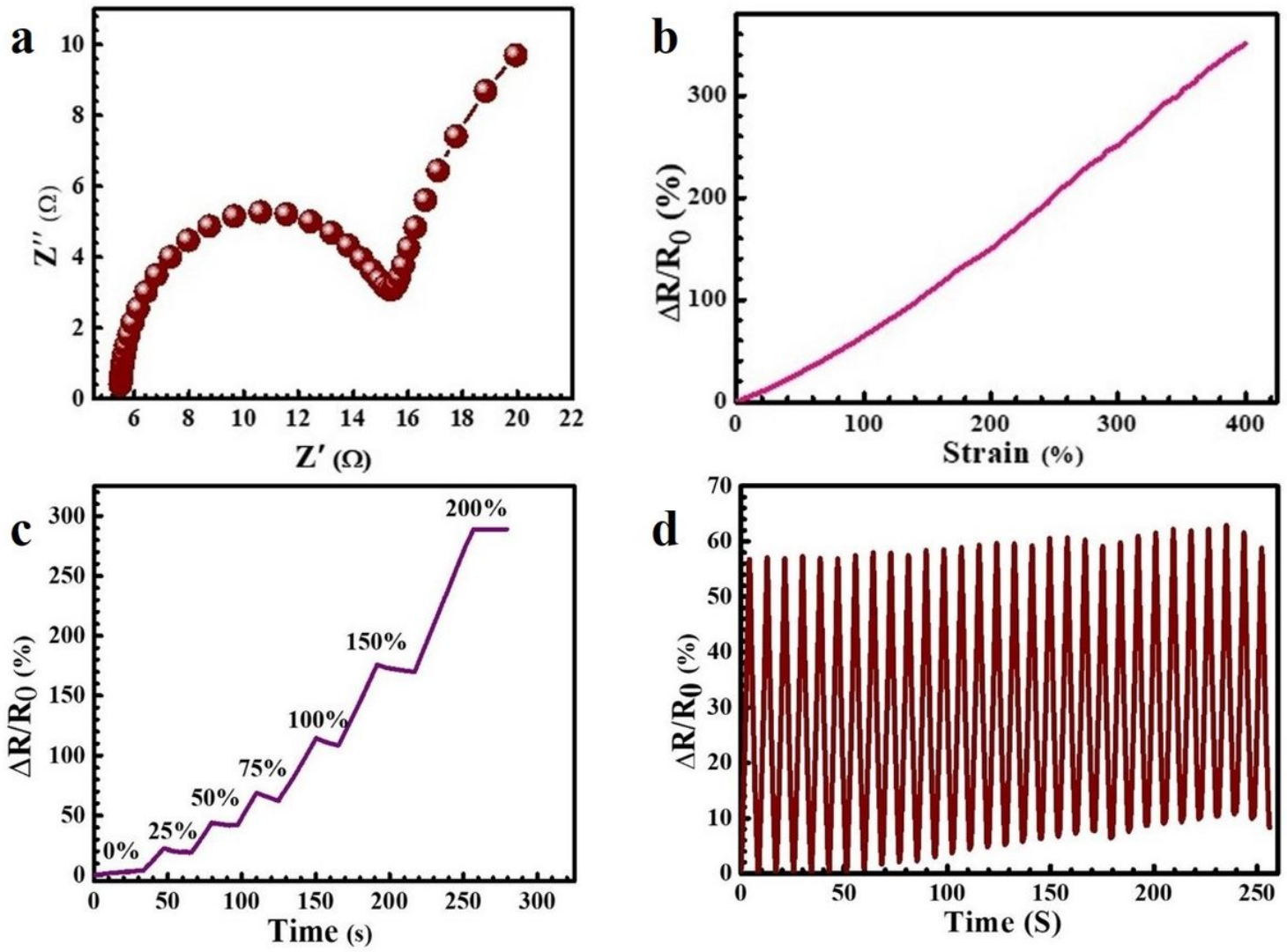

Figure 9

(a) EI spectrum of hydrogel; (b) change in resistance vs change in strain (%); (c) relative change in resistance at different strain (%) as a function of time; and (d) change in relative resistance vs time (50%, 30 cycles).

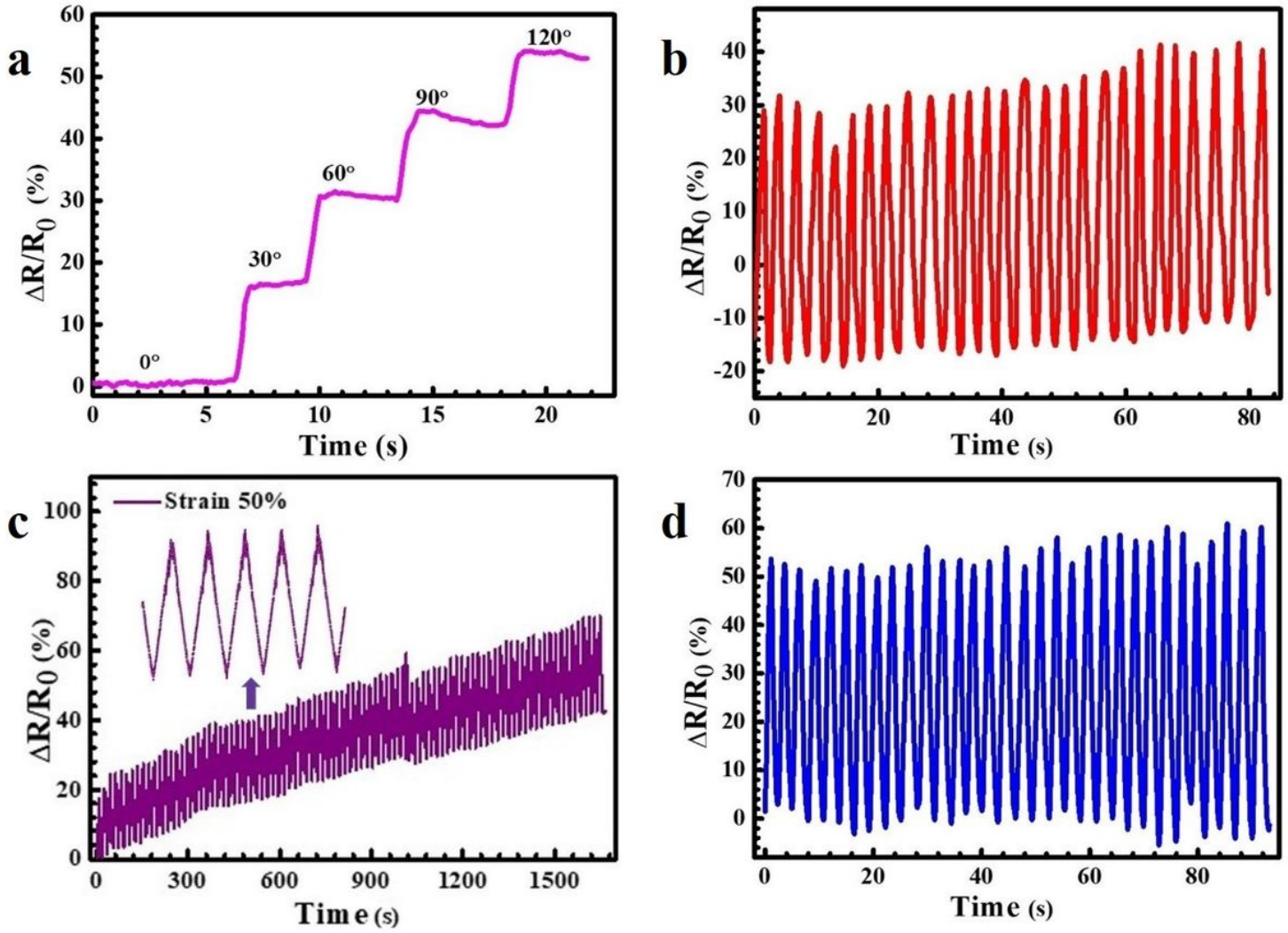

Figure 10

Application of hydrogel sensor in the monitoring of various human motion as a relative change in resistance versus time, (a) the motion of forefinger at different angles; (b) cyclically bending on the finger; (c) 50% strain (100 cycles), and (d) cyclically bending and releasing of the hydrogel sensor on the wrist.

Supplementary Files

This is a list of supplementary files associated with this preprint. Click to download.

- Schema1.jpeg
- ElectronicSupplementaryInformation.docx